PHYSICAL REVIEW D VOLUME 47, NUMBER 5 1 MARCH 1993

ARTICLES

Particle production in interactions of 200 GeV/nucleon oxygen and sulfur nuclei in nuclear emulsion

A. Dąbrowska, R. Hołyński, A. Jurak, A. Olszewski, M. Szarska, A. Trzupek, B. Wilczyńska, H. Wilczyński, W. Wolter, B. Wosiek, and K. Woźniak
Institute of Nuclear Physics, Kawiory 26A, 30-055 Kraków, Poland

M. L. Cherry, W. V. Jones, K. Sengupta, and J. P. Wefel
Department of Physics and Astronomy, Louisiana State University, Baton Rouge, Louisiana 70803

P. S. Freier* and C. J. Waddington
School of Physics and Astronomy, University of Minnesota, Minneapolis, Minnesota 55455

(KLM Collaboration)

(Received 7 August 1992)

Oxygen and sulfur nuclei with energies of 200 GeV/nucleon have been allowed to interact in nuclear emulsions exposed at CERN. These emulsions have been scanned with a minimum bias so that essentially all the interactions occurring were detected. Nearly 1000 interactions of each projectile have been analyzed. We present results on the multiplicity distributions, the pseudorapidity distributions, and the fragmentation of the projectile and target nuclei. It is shown that the mean number of intranuclear collisions in each interaction, calculated from a superposition model, provides a useful parameter for organizing the data. We conclude that there are no significant deviations even at these energies from models, such as the VENUS model, describing the interactions as being the superposition of individual nucleon-nucleon collisions.

PACS number(s): 25.75.+r, 12.40.Aa, 13.85.Hd, 25.40.Ve

I. INTRODUCTION

The interactions of relativistic nuclei with target nuclei have been studied by numerous authors using a variety of experimental techniques; see, e.g., [1,2]. During the exploratory phase of these studies, as the available energy of the projectile nuclei increased, the nuclear emulsion technique has provided a global view of the phenomena that occur, a view whose 4π acceptance and fine spatial resolution are complementary to other techniques that provide specific data with higher statistical significance.

The principal goal of the studies of high-energy nucleus-nucleus interactions has been the search for the phase transition predicted by QCD [3–7] or for other collective effects. Observations of nonstatistical fluctuations [8–11] may indeed signal the occurrence of new phenomena. On the other hand, it has been known for many years that superposition models adequately describe hadron-nucleus interactions [12–14]. Superposition incorporates a wide class of models (e.g., VENUS [15] and FRITIOF [16]) in which the main parameter governing the particle production is the number of individual nucleon-nucleon collisions. It is anticipated, however, that these superposition models may begin to fail and new physics may appear as the projectile mass and energies are increased. Yet the studies of the global characteristics of nucleus-nucleus interactions with the currently available projectiles and energies seem to confirm the validity of these models. This may mean that either collective effects are very rare or their influence on the global properties of interactions is weak.

In this paper we present some of the results obtained from the CERN experiment EMU07 in which nuclear emulsions were exposed to oxygen (^{16}O) and sulfur (^{32}S) beams with an energy of 200 GeV/nucleon. These results have concentrated on obtaining a global view of the inelastic interactions by attempting to detect an unbiased sample of all the interactions. The characteristics of these minimum bias samples as well as of subsamples with different impact parameters are presented. It is shown that the superposition model is essentially valid over the whole range of the number of elementary intranuclear nucleon-nucleon collisions occurring in these interactions. It was possible to reach this conclusion because the nuclear emulsion technique provides us with a relatively simple and efficient trigger for selecting events on the basis of their impact parameter on the target nuclei.

*Deceased.

II. EXPERIMENTAL

Stacks composed of BR-2 nuclear emulsion pellicles with dimensions of 5×10 cm^2 and 600 μm thick were exposed at CERN to the 200 GeV/nucleon ^{16}O and ^{32}S beams. These stacks were oriented so that the beams were parallel to the pellicles. The emulsions were developed with a minimum ionization of approximately 28 grains/100 μm, and then analyzed with optical microscopes. An along-the-track minimum bias scan was performed. The interaction mean free paths in emulsion were determined and were found to be (12.3 ± 0.3) cm and (8.5 ± 0.2) cm for oxygen and sulfur primaries, respectively. These experimentally obtained values are in good agreement with those calculated using the predicted cross sections published in [17] or [18] and the known composition of BR-2 nuclear emulsion [19]. Consequently, the efficiency of detecting interactions during the scanning must have been very high even for those interactions with low multiplicities.

In the following we will deal only with those interactions in which at least one particle was produced. Pure nuclear fragmentation or electromagnetic dissociation of at least one of the two colliding nuclei were rejected. The data samples contained 868 interactions of oxygen and 929 interactions of sulfur.

Interactions were analyzed by studying the tracks emitted from each interaction detected. These tracks were classified according to the commonly accepted emulsion experiment terminology, based upon their ionization and measured properties. We defined the following groups of tracks.

N_Z—Multicharged projectile fragments are defined as tracks due to relativistic nuclei with $Z \geq 2$. Typically we determine the number of α particles, N_α, and the number of fragments, N_F, with charge $Z > 2$, separately.

N_s—Shower particles (fast particles with $\beta > 0.7$) are defined as tracks with ionization $I < 1.4I_0$ where I_0 is the minimum ionization produced by a singly charged particle. This group includes tracks due to particles produced in the interactions as well as those singly charged particles, predominantly protons, released from the projectile nucleus or knocked off from the target nucleus.

N_g and N_b—Grey and black tracks (which are often combined into a single group of heavy tracks, N_h) are tracks formed by slower ($\beta < 0.7$) heavily ionizing ($I > 1.4I_0$) particles emitted from the struck target nucleus. Grey tracks are mostly recoil protons with energies from 30 to 400 MeV, with a small number of heavier hydrogen isotopes and a few percent admixture of low-momentum pions. The black tracks are produced by low-energy singly and multicharged target fragments. The experimental separation between black and grey tracks is somewhat subjective. We have based it on the criterion that the track should have an ionization that is greater (black), or less (grey), than that of a 30 MeV proton. This corresponds to a grain density of about eight times minimum and a residual range for a proton of 3 mm in emulsion. Since only a few of the tracks in this group are ambiguous, the slightly subjective nature of the separation criteria does not affect our analysis and conclusions significantly.

For each multicharged projectile fragment, shower particle, and heavily ionizing particle emitted from the interaction vertex, the emission angle θ (the polar angle of the track with respect to the direction of the primary ^{16}O or ^{32}S ion track) was determined under high magnification in the microscope. The angles of shower particles were measured with an accuracy of ~ 0.1 in pseudorapidity $[\eta = -\ln\tan(\theta/2)]$, which required increasing accuracy as θ became smaller. The angles of the black and grey tracks were measured with an accuracy of less than 1°. The charges of the projectile fragments with $Z > 2$ were determined by counting a sufficient number of δ rays to determine the charge with a standard deviation of about 0.5 of a charge unit. The helium nuclei were identified from their ionization and lack of multiple scattering; the identification was essentially unambiguous.

These data for oxygen and sulfur interactions have been compared with those obtained earlier from the analysis of 2595 proton-emulsion interactions [20,21] at the same primary energy of 200 GeV.

III. CENTRALITY OF COLLISIONS

The analyzed data samples of oxygen and sulfur interactions have been divided into groups of events characterized by different degrees of centrality, a quantity which can be related to the value of the impact parameter of nucleus-nucleus collisions. We have chosen to represent the degree of centrality by the number, $N_{\rm coll}$, of intranuclear nucleon-nucleon collisions, a parameter that is an essential part of any superposition model and which allows us to organize the data in a coherent fashion. For each interaction one can determine the forward charge $Q_F(\theta_c)$ as the absolute value of the total charge emitted within the very forward cone of half-angle θ_c , i.e.,

$$Q_F(\theta_c) = \sum Z_F + 2N_\alpha + N_s(\theta_c) \qquad (1)$$

where ΣZ_F is the sum of charges of all N_F projectile fragments with charge $Z > 2$, N_α is the number of alpha particles, and $N_s(\theta_c)$ denotes the number of singly charged shower particles within the forward cone of half-angle θ_c.

Forward charge $Q_F(\theta_c)$ would be equal to the total charge carried by noninteracting projectile nucleons, if $N_s(\theta_c)$ included only spectator protons. However, independently of the choice of θ_c, $N_s(\theta_c)$ is contaminated by produced particles. Thus, we attempted to choose such a cone in which all spectator protons are contained and the number of produced particles is as small as possible. Comparing experimentally obtained Q_F values with the calculated ones from the VENUS[1] Monte Carlo model of nucleus-nucleus interactions [15] we find that for interactions at 200 GeV/nucleon a choice of $\theta_c = 3$ mrad represents our best compromise to the requirements above.

[1]In our calculations we used version 3.12 of the VENUS model.

This is the same value as that adopted by other emulsion groups analyzing similar data [22,23]. We have compared in Fig. 1 our experimental probability distributions of Q_F for $\theta_c = 3$ mrad with the model distributions from the VENUS program for oxygen and sulfur interactions. With the exception of the relatively small inconsistencies in the region of large Q_F values (peripheral collisions), which are probably due to uncertainties in the charge measurements of heavy projectile fragments, there is generally good agreement between the data and the model predictions. Decreasing the assumed value of θ_c worsens the agreement.

This agreement justifies the use of the VENUS model to relate the experimentally measured values of Q_F with the calculated mean number $\langle N_{\rm coll}\rangle$ of intranuclear nucleon-nucleon collisions. The relation between $\langle N_{\rm coll}\rangle$ and Q_F is shown in Fig. 2 for both oxygen and sulfur interactions in emulsion. Using this relation we can assign a value of $\langle N_{\rm coll}\rangle$ to every event on the basis of the measured value of Q_F . It can be seen that the maximum values of $\langle N_{\rm coll}\rangle$ for oxygen and sulfur interactions in emulsion are about 60 and 120 collisions, respectively. These values are for the most central events, those with minimum Q_F, and since they greatly exceed the mass numbers of the projectile nuclei, they imply, as does the VENUS model, that some of the projectile nucleons interact several times during their passage through the average target nucleus. As a consequence, these interactions cannot be characterized as all being due to nucleons with the incident energy of the projectile nucleons. Some must be secondary and between nucleons with less than the initial energy.

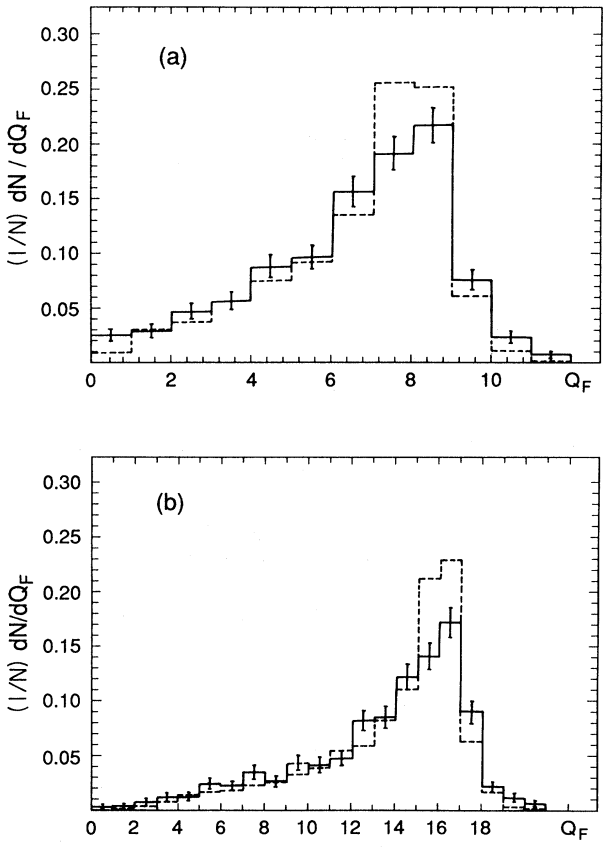

FIG. 1. The probability distribution of total charge Q_F, within the forward cone of half-angle $\theta_c = 3$ mrad, for (a) oxygen and (b) sulfur interactions in emulsion. The experimental data, shown by the solid histogram with statistical errors, is compared to the predictions of the VENUS model shown by the dashed histogram.

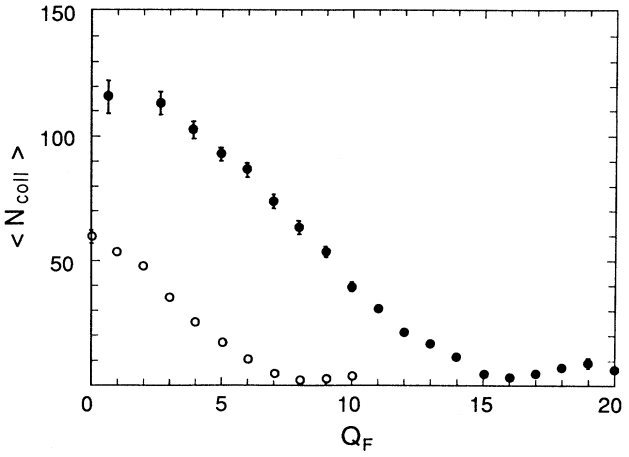

FIG. 2. The relation derived from the VENUS model between the mean number $\langle N_{\rm coll}\rangle$ of intranuclear nucleon-nucleon collisions and the charge Q_F for oxygen (○) and sulfur (●) interactions in emulsion. The errors shown are from the finite numbers of events generated by the VENUS program.

IV. MULTIPLICITY OF PRODUCED PARTICLES

The multiplicity of produced charged particles is defined as

$$N_\pi = N_s - \left[Z_P - (2N_\alpha + \sum Z_F)\right] \quad (2)$$

where Z_P represents the charge of the projectile. Using this definition, singly charged projectile fragments (spectator protons) as well as protons from the projectile which interacted, are subtracted from the total number N_s of shower particles observed. This quantity N_π can be determined experimentally and is predicted by the VENUS program (see Table I).

TABLE I. The mean multiplicities of shower N_s and produced N_π particles for oxygen and sulfur interactions in emulsion at 200 GeV/nucleon, including the VENUS model predictions.

Projectile	Sample	$\langle N_s\rangle$	$\langle N_\pi\rangle$	$\langle N_\pi\rangle_{\rm VENUS}$
^{16}O	868	63.0 ± 2.1	58.4 ± 2.1	60.3 ± 1.0
^{32}S	929	87.8 ± 3.3	79.5 ± 3.1	85.3 ± 1.4

The experimental and predicted probability distributions for oxygen and sulfur interactions are shown in Fig. 3. The distribution of N_π for sulfur interactions reaches much larger values than that for oxygen and extends up to about 400 charged particles. The predictions of the VENUS model are in satisfactory agreement with the experimental data except for the very high multiplicity region where the yield predicted by the VENUS model is higher than that observed. This discrepancy concerns less than 2% of the total number of interactions for both the oxygen and sulfur projectiles. However, it does suggest that this version of the VENUS model overestimates the large multiplicity tail. We will see later that this is also confirmed by the analysis to follow.

In Fig. 4 we present the dependence of the measured mean multiplicity $\langle N_\pi \rangle$ on the mean number $\langle N_{\rm coll} \rangle$ of intranuclear nucleon-nucleon collisions for inclusive interactions of proton, oxygen, and sulfur projectiles with nuclear emulsion at 200 GeV/nucleon. One can calculate $\langle N_{\rm coll} \rangle$ for inclusive interactions from simple geometrical Glauber type calculations assuming the cross sections for

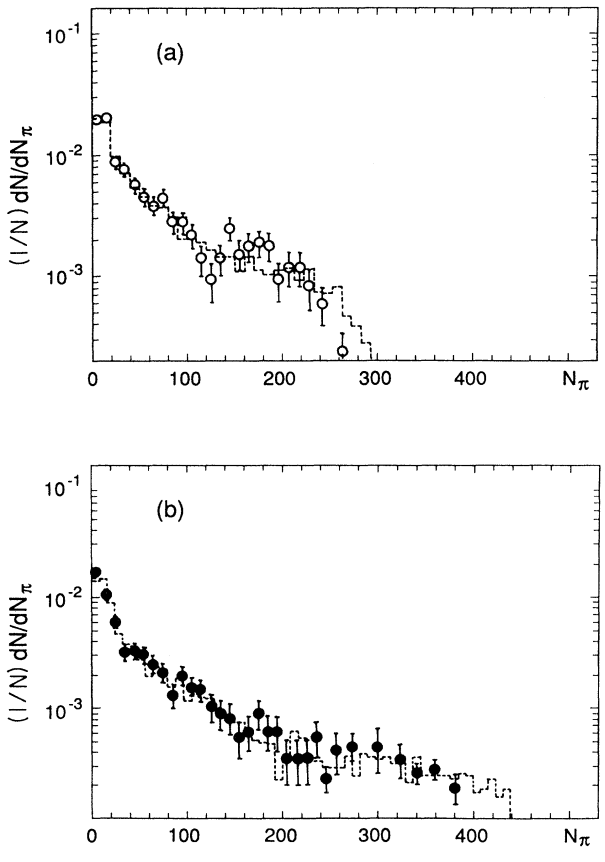

FIG. 3. The probability distribution of the produced particle multiplicity, N_π for (a) oxygen (○) and (b) sulfur (●) interactions in emulsion shown with the statistical errors. The predictions of the VENUS model are shown as the dashed histogram, which would have sampling errors $\sqrt{5}$ times smaller than the statistical errors shown.

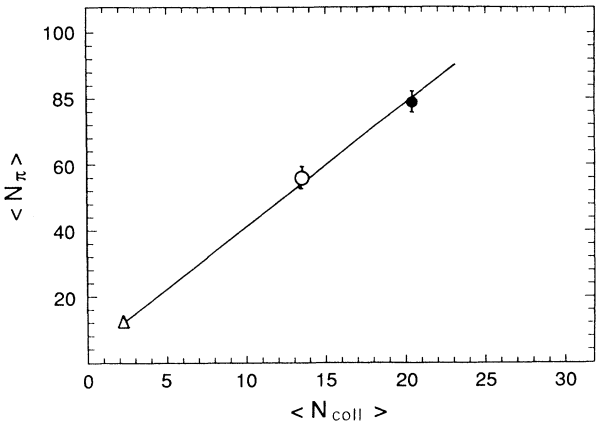

FIG. 4. The dependence of the mean multiplicity $\langle N_\pi \rangle$ on $\langle N_{\rm coll} \rangle$ for proton (△), oxygen (○), and sulfur (●) interactions in emulsion. The straight line is a linear fit to the data and gives Eq. (3).

the various components of emulsion. The three points in Fig. 4 then define a linear relation between the two parameters of the form

$$\langle N_\pi \rangle = (3.78 \pm 0.15)\langle N_{\rm coll} \rangle + (4.14 \pm 0.39). \quad (3)$$

In order to study the observed multiplicities in oxygen and sulfur interactions in more detail, we divided our samples of oxygen and sulfur interactions into subgroups characterized by different values of $\langle N_{\rm coll} \rangle$ for intranuclear nucleon-nucleon collisions. To do this we applied the procedure described in Sec. III. Using the relation between Q_F and $\langle N_{\rm coll} \rangle$ (see Fig. 2), the samples of oxygen and sulfur interactions were divided into groups of collisions with different degree of centrality. This procedure makes it possible to extend the analysis to significantly larger values of $\langle N_{\rm coll} \rangle$ than in Fig. 4 for the full inclusive data set.

The relation between the mean multiplicity $\langle N_\pi \rangle$ and the corresponding mean number of collisions $\langle N_{\rm coll} \rangle$ is shown in Fig. 5 for both projectiles. The straight line represents Eq. (3). It is seen that the oxygen and sulfur data can be described by this equation for values of $\langle N_{\rm coll} \rangle$ less than about 30. However, for higher values of $\langle N_{\rm coll} \rangle$ the values of $\langle N_\pi \rangle$ are smaller than predicted. This may be a consequence of the effects of the lower energies of secondary and later nucleon-nucleon interactions in central collisions with heavy target nuclei (Ag, Br), which will become progressively more important as $\langle N_{\rm coll} \rangle$ increases.

It is interesting to compare the above results with similar ones for proton-nucleus interactions. The relation between $\langle N_\pi \rangle$ and $\langle N_{\rm coll} \rangle$ for proton interactions at 200 GeV is shown in Fig. 6. Note the very small range of $\langle N_{\rm coll} \rangle$ for these interactions. Two sets of data are presented: the proton-emulsion interactions [20,21] divided into subgroups with different $\langle N_{\rm coll} \rangle$ using the method described in Ref. [24] and the results from an electronic experiment [25] performed on different targets (carbon, emulsion, copper, silver, and lead). For these relatively

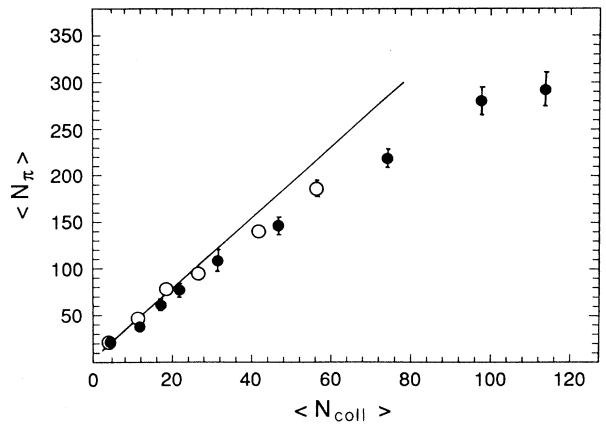

FIG. 5. The relation between the values of $\langle N_\pi \rangle$ and $\langle N_{\rm coll} \rangle$ for groups of events with selected values of the forward charge Q_F for oxygen (○) and sulfur (●) interactions. The straight line represents Eq. (3).

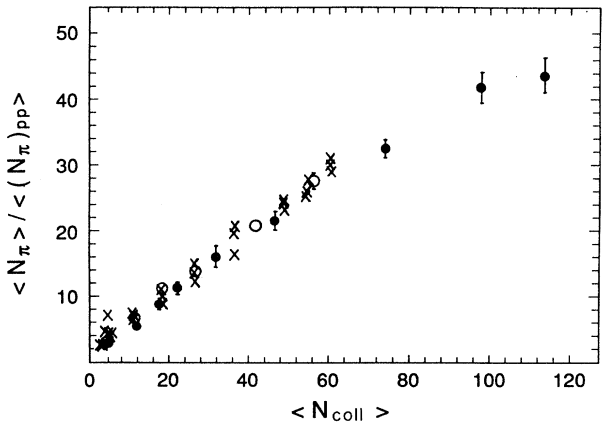

FIG. 7. The dependence of the normalized mean multiplicity $\langle N_\pi \rangle / \langle (N_\pi)_{pp} \rangle$ on $\langle N_{\rm coll} \rangle$ for oxygen (○) and sulfur (●) interactions in emulsion at 200 GeV/nucleon. The data published in [26] for oxygen interactions in emulsion at 14.5, 60, and 200 GeV/nucleon are shown by ×.

small values of $\langle N_{\rm coll} \rangle$, Eq. (3) provides very good agreement with the data.

Finally, we have looked at the normalized mean multiplicity in nucleus-nucleus collisions, M, defined by $M = \langle N_\pi \rangle / \langle (N_\pi)_{pp} \rangle$ [where $\langle (N_\pi)_{pp} \rangle$ stands for the mean produced charged particle multiplicity in inclusive proton-proton collisions at the same energy per nucleon]. This quantity has been plotted as a function of $\langle N_{\rm coll} \rangle$ for our sample of oxygen and sulfur data at 200 GeV/nucleon in Fig. 7. In the same figure the data from interactions of oxygen projectiles at 14.5, 60, and 200 GeV/nucleon reported previously [26] are also shown. No systematic mass or energy dependence can be seen in Fig. 7. All the data seem to follow a common linear relation, apart from events with very large $\langle N_{\rm coll} \rangle$—those which are the very central collisions of sulfur with Ag, Br nuclei—for which M is less than expected by extrapolation.

The common linear dependence of the scaled multiplicity over a wide range of the number of intranuclear nucleon-nucleon collisions, irrespective of the mass of the projectile and its energy, strongly supports the idea that the number of collisions is a good parameter to describe the particle production.

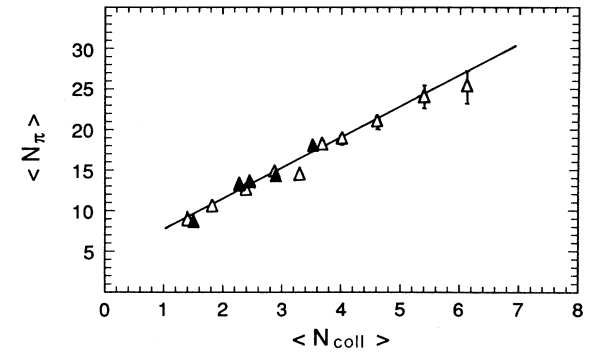

FIG. 6. The relation between the values of $\langle N_\pi \rangle$ and $\langle N_{\rm coll} \rangle$ for proton-nucleus interactions: Inclusive interactions in order of increasing $\langle N_{\rm coll} \rangle$ with C, emulsion, Cu, Ag, and Pb nuclei [25] are shown by ▲. Proton interactions in emulsion separated into subgroups with different values of $\langle N_{\rm coll} \rangle$ are shown by △. The straight line represents Eq. (3). Note the very narrow range of $\langle N_{\rm coll} \rangle$ here compared with that in Fig. 5.

V. PSEUDORAPIDITY DISTRIBUTIONS OF SHOWER PARTICLES

The pseudorapidity ($\eta = -\ln \tan \theta/2$) distributions for central collisions of oxygen projectiles at 14.6, 60, and 200 GeV/nucleon were analyzed by us earlier [27]. The inclusive pseudorapidity distributions of shower particles N_s, produced in proton, oxygen, and sulfur interactions in nuclear emulsion are shown in Fig. 8. The areas un-

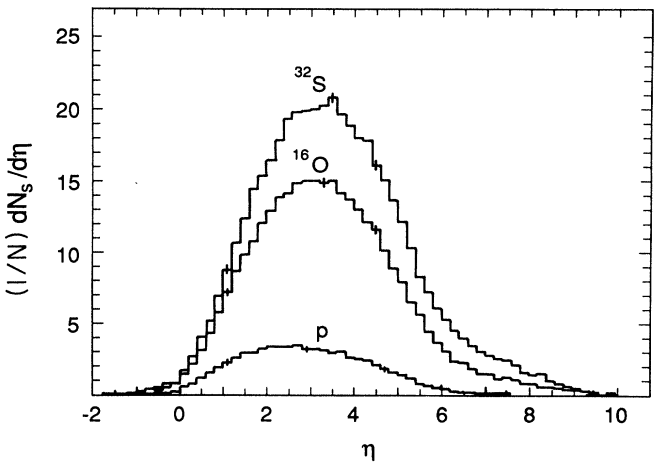

FIG. 8. The inclusive pseudorapidity distributions of shower particles, N_s, produced in proton, oxygen, and sulfur interactions in emulsion.

TABLE II. Experimental and VENUS model predictions of the mean values and the dispersion of pseudorapidity distributions of shower particles N_s for oxygen, sulfur, and proton interactions in emulsion at 200 GeV/nucleon.

	Experiment		VENUS model	
Projectile	$\langle\eta\rangle$	σ_η	$\langle\eta\rangle$	σ_η
^{16}O	3.23 ± 0.01	1.520 ± 0.004	3.177 ± 0.002	1.475 ± 0.002
^{32}S	3.37 ± 0.01	1.558 ± 0.004	3.295 ± 0.002	1.464 ± 0.001
p	2.86 ± 0.01	1.489 ± 0.005	2.884 ± 0.006	1.554 ± 0.004

der the histograms represent the average multiplicities of shower particles and illustrate the dependence of the average multiplicities on atomic mass of the projectile. The increase of particle production in heavy ion interactions relative to the proton induced reactions is evident over the entire range of pseudorapidity. In Table II we present the experimental and the VENUS model predictions of the mean values and dispersions of the pseudorapidity distributions of shower particles N_s. The mean value of η increases with the increasing mass of the projectile, both for experimental data and the VENUS model predictions. The pseudorapidity distributions for interactions with different values of $\langle N_{\rm coll}\rangle$, selected from the appropriate intervals of Q_F (see Table III), are plotted in Fig. 9 for oxygen and sulfur projectiles. One can see that the average multiplicity $\langle N_s\rangle$ depends strongly on the number of intranuclear nucleon-nucleon collisions and that the mean value of pseudorapidity, $\langle\eta\rangle$, shown by the black dots in Fig. 9, decreases with the increasing centrality of the collision. The numerical values of $\langle N_s\rangle$ and $\langle\eta\rangle$ are listed in Table III.

It is shown in Fig. 5 that the mean multiplicities $\langle N_\pi\rangle$ in oxygen-emulsion and sulfur-emulsion interactions depend mainly on the average number $\langle N_{\rm coll}\rangle$ of intranuclear nucleon-nucleon collisions and not on the atomic mass of the projectile. To study this feature in more detail we have compared the pseudorapidity distributions for oxygen and sulfur interactions characterized by closely similar values of $\langle N_{\rm coll}\rangle$. These comparisons are shown in Fig. 10 for three different selections of $\langle N_{\rm coll}\rangle$ (see Table III). We can conclude from these comparisons that the angular distributions of the shower particles from oxygen and sulfur interactions are essentially, but not entirely, the same for groups of events characterized by similar values of collisions $\langle N_{\rm coll}\rangle$. The observed small differences can be explained by the fact that the same value of $\langle N_{\rm coll}\rangle$ can be realized by different combinations of projectile and target nucleons participating in the intranuclear nucleon-nucleon collisions.

An alternative way of presenting these distributions is to study the variation of the pseudorapidity density of the shower particles, $\rho(\eta)$, with $\langle N_{\rm coll}\rangle$, where

$$\rho(\eta) = \frac{1}{N}\frac{dN_s}{d\eta}. \tag{4}$$

The densities $\rho(\eta)$ for three intervals of η are given in Fig. 11 both for oxygen and sulfur interactions. The dependence of $\rho(\eta)$ on $\langle N_{\rm coll}\rangle$ in all three of the intervals can be satisfactorily fitted by linear relations, where the slight projectile mass dependences are a reflection of the differences seen in the distributions shown in Fig. 10.

These pseudorapidity densities for nucleus-nucleus interactions can be normalized by using the proton data for nucleon-nucleon interactions. A measure of the enhancement of particle production in different pseudorapidity bins in nucleus-nucleus interaction is the ratio

$$R(\eta) = \rho_A(\eta)/\rho_p(\eta) \tag{5}$$

where $\rho_A(\eta)$ and $\rho_p(\eta)$ denote the particle densities in nucleus-nucleus and proton-proton collisions respectively, at the same primary energy. The ratio $R(\eta)$ for oxygen and sulfur interactions in emulsion as a function of η is depicted in Fig. 12. In the pseudorapidity region $-2 < \eta < 6.5$ the parameter R depends only weakly on η. (The range of pseudorapidities above 6.5 is strongly dominated

TABLE III. The mean number $\langle N_{\rm coll}\rangle$ of intranuclear nucleon-nucleon collisions selected according to the forward charge flow Q_F for oxygen and sulfur interactions in emulsion. The mean numbers of $\langle N_s\rangle$ and $\langle\eta\rangle$ are also given.

Projectile	Sample	Q_F	$\langle N_{\rm coll}\rangle$	$\langle N_s\rangle$	$\langle\eta\rangle$
^{16}O	(1)	7–10	4.3	24.5 ± 1.3	3.42 ± 0.02
^{16}O	(2)	4–6	17.3	74.8 ± 3.0	3.30 ± 0.01
^{16}O	(3)	0–3	45.8	164.3 ± 5.0	3.18 ± 0.01
^{32}S	(1)	15–22	4.6	27.7 ± 1.6	3.56 ± 0.02
^{32}S	(2)	12–14	16.1	65.5 ± 3.3	3.50 ± 0.01
^{32}S	(3)	8–11	44.1	153.0 ± 6.6	3.38 ± 0.01
^{32}S	(4)	4–7	94.2	272.1 ± 9.1	3.26 ± 0.01
^{32}S	(5)	0–3	114.0	309.2 ± 17.2	3.10 ± 0.02

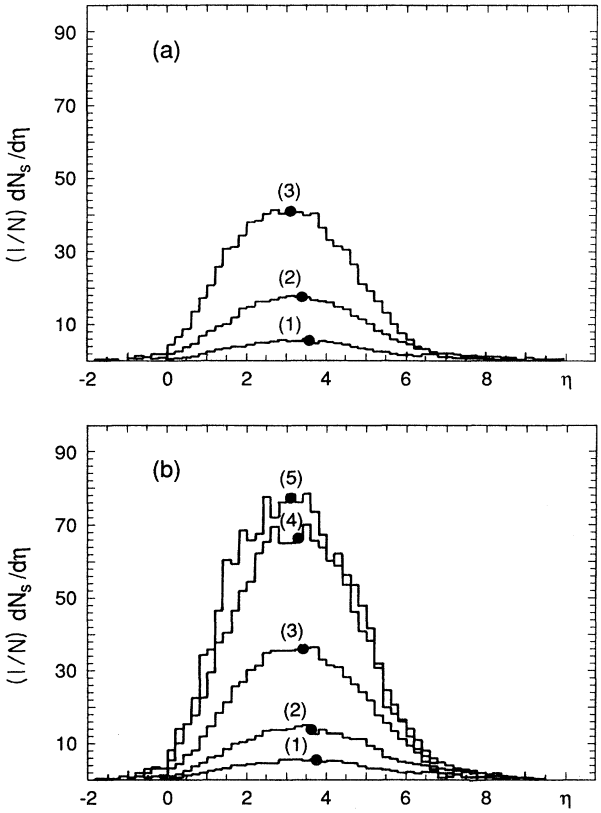

FIG. 9. The pseudorapidity distributions for (a) oxygen and (b) sulfur interactions with the different values of $\langle N_{\rm coll}\rangle$ listed in Table III. The mean values $\langle\eta\rangle$ of pseudorapidity are marked by dots.

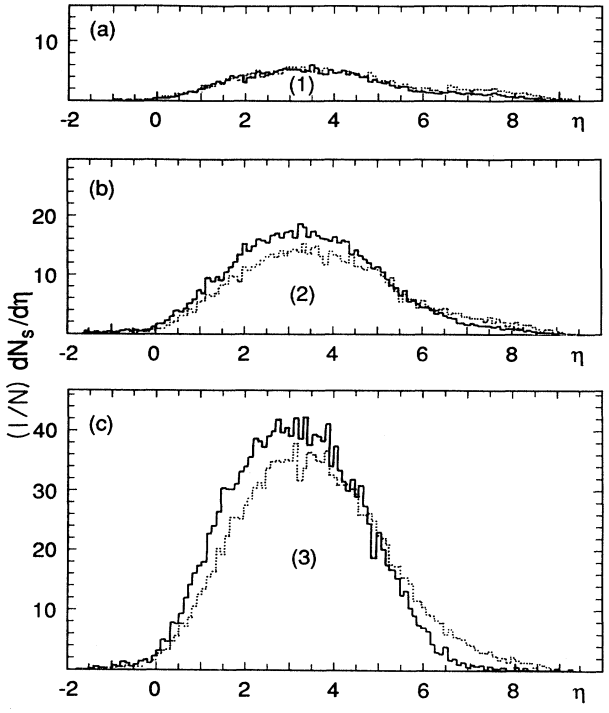

FIG. 10. Comparison between the pseudorapidity distributions of shower particles N_s produced in oxygen (solid histogram) and sulfur (dotted histogram) interactions for three subsamples characterized by different values of $\langle N_{\rm coll}\rangle$ (see Table III).

by spectator protons and is not relevant to considerations of the produced particle multiplicities.)

VI. FRAGMENTATION OF THE PROJECTILE NUCLEUS

We have already presented the projectile fragmentation data for the oxygen primaries as a function of the energy of the incident beam [28] and have found that the yield of fragments increases significantly as the energy increases. This increase can be related to the growth of the cross-section for electromagnetic dissociations at these very high energies.

The data presented here are restricted to the interactions in which the fragmentation of 200 GeV/nucleon oxygen and sulfur projectiles is associated with the particle production. Thus, they include neither the electro-

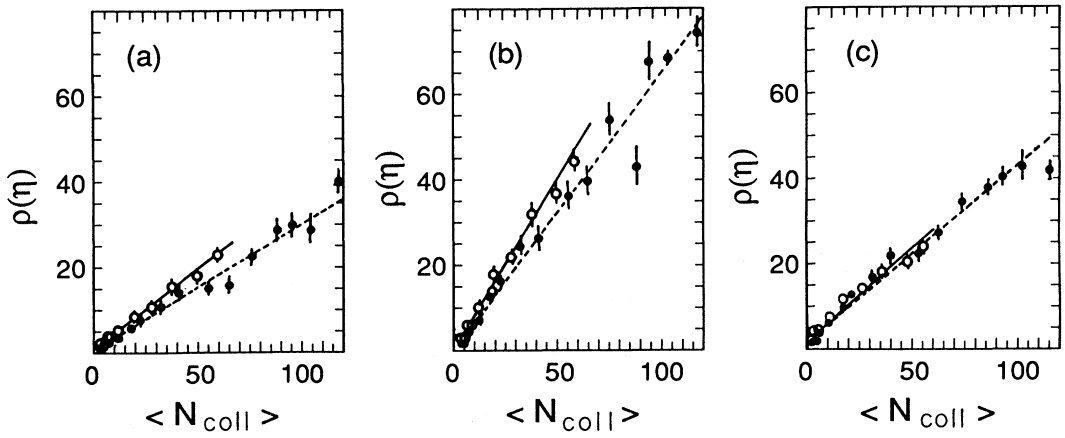

FIG. 11. The density $\rho(\eta)$ of the pseudorapidity distributions as a function of $\langle N_{\rm coll}\rangle$ for three different intervals of η: (a) $0 \le \eta < 2$, (b) $2 \le \eta < 4$, (c) $4 \le \eta < 6$, for oxygen (○) and sulfur (●) interactions. The solid line and dashed line are linear fits to the two sets of data.

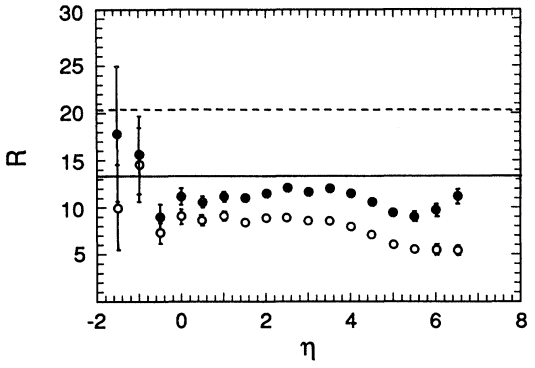

FIG. 12. Normalized particle densities R as a function of pseudorapidity η for oxygen (○) and sulfur (●) interactions. Solid and dashed lines indicate the R values corresponding to $\langle N_{\text{coll}} \rangle$ for oxygen and sulfur interactions respectively.

magnetic dissociation nor the pure nuclear fragmentation processes and therefore the results given below cannot be compared with previously published results [28].

The probability distributions of charge Z_F of the heavy fragments and α particles emitted in sulfur and oxygen interactions are presented in Fig. 13. For comparison with these data we have also considered an extensive data set of 4154 interactions of ^{22}Ne projectiles with an energy of 4.2 GeV/nucleon [29]. The Z_F distribution for this set is shown.

The measured percentage probabilities for the different modes of fragmentation are summarized in Table IV. A number of conclusions can be drawn from Table IV and

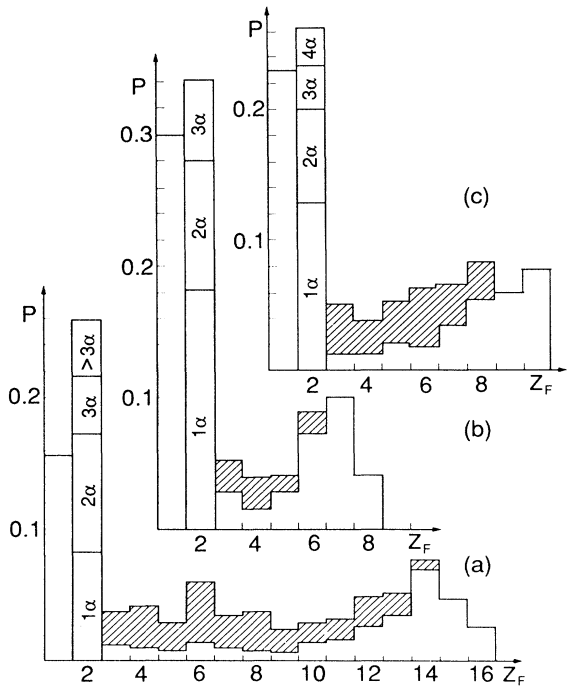

FIG. 13. The probability P of fragmentation of (a) sulfur, (b) oxygen, and (c) neon projectiles into fragments with charge Z_F, for interactions in emulsion. The shadowed area represents the probability for a given fragment Z_F to be accompanied by α particle(s). $Z_F = 1$ denotes events without α particle(s) or heavier fragments. In the case of fragmentation into α particles only the number of α fragments is indicated.

TABLE IV. Some parameters describing the projectile fragmentation for inelastic interactions of oxygen, neon, and sulfur in emulsion.

	^{16}O 200 GeV/n	^{22}Ne 4.2 GeV/n	^{32}S 200 GeV/n
Fragmentation Mode	Probability (in percent) for different fragmentation modes		
Two fragments with $Z > 2$	0.1 ± 0.1	1.0 ± 0.2	2.0 ± 0.5
One fragment with $Z > 2$	36 ± 2	50 ± 1	56 ± 2
Fragment(s) with $Z > 2$ and no α particles	29 ± 2	29 ± 1	31 ± 2
Fragment(s) with $Z > 2$ and α particle(s)	7 ± 1	21 ± 1	28 ± 2
α particles and no heavier fragments	34 ± 2	26 ± 1	26 ± 2
No multiply charged fragment	30 ± 2	23 ± 1	16 ± 1
	The mean number of multicharge fragments per event		
Fragments with $Z > 2$	0.36 ± 0.02	0.50 ± 0.01	0.61 ± 0.02
α particles	0.61 ± 0.03	0.72 ± 0.01	0.96 ± 0.04
	The mean charge of the fragment		
Fragments with $Z > 2$	5.7 ± 0.1	6.9 ± 0.1	9.6 ± 0.2
Fragments with $Z > 2$ and no α particles	6.1 ± 0.1	7.8 ± 0.1	11.6 ± 0.2
Fragments with $Z > 2$ and α particle(s)	4.2 ± 0.1	5.4 ± 0.1	7.4 ± 0.2

Fig. 13. As the mass of the projectile increases we note the following.

Firstly, the probability of producing a single fragment with no accompanying α particles is independent of mass and energy. The observed increase in the probability of producing a fragment is entirely due to those fragments that are accompanied by α particle(s).

Secondly, the probability that only α particles but no heavier fragments are produced decreases. However, since low-energy neon and high-energy sulfur have the same probability of producing only α particles it would appear that this mode may increase with increasing energy.

Thirdly, there is a rapid decrease in the number of events with no multiply charged fragments.

Fourthly, the mean number of fragments and α particles as well as the mean charge of the fragments all increase.

Finally, the probability of producing multiple fragments with $Z > 2$ in a collision is always small but increases very rapidly with increasing mass, which is consistent with the large numbers of multiple fragments, observed in interactions of low-energy (≤ 1.0 GeV/nucleon) ^{179}Au nuclei in emulsion [30].

VII. FRAGMENTATION OF THE TARGET NUCLEUS

Due to the collision with the projectile, the target nucleus becomes excited and fragments. The process of the fragmentation of the target nucleus can be investigated by analyzing the grey (N_g) and black (N_b) tracks (defined in Sec. II) of the particles emitted from the struck nucleus. In Table V we present the mean values of N_g and N_b in oxygen and sulfur interactions with nuclear emulsion.

We have also included in this table the corresponding quantities for proton interactions [20,21]. In Fig. 14 the multiplicity distributions of grey and black tracks from oxygen and sulfur interactions are compared with those of proton interactions. From Fig. 14 we can see that the distribution of black tracks is, essentially, independent

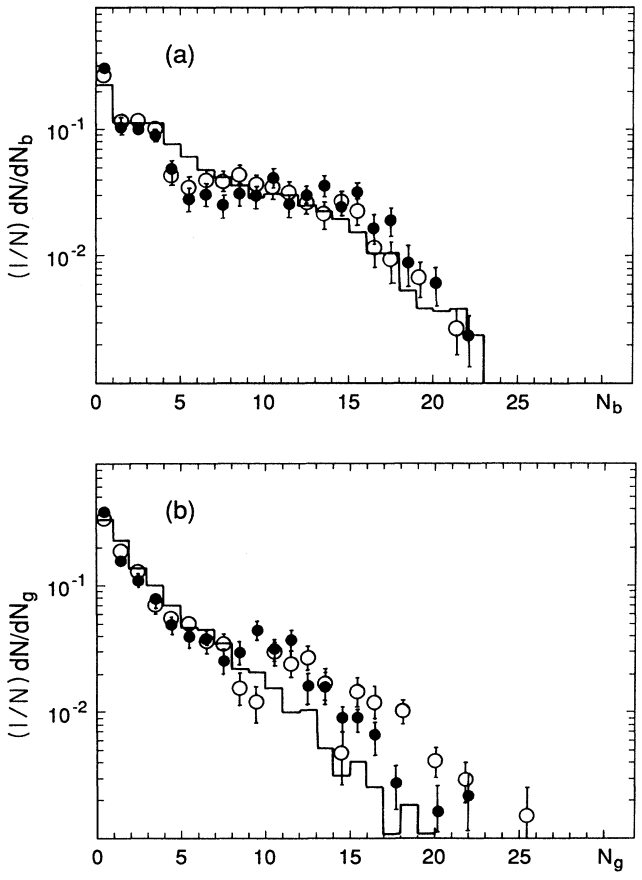

FIG. 14. The multiplicity distributions of (a) black N_b tracks and (b) grey N_g tracks for oxygen (○) and sulfur (●) interactions. For comparison the distribution for proton interactions is shown by the histogram.

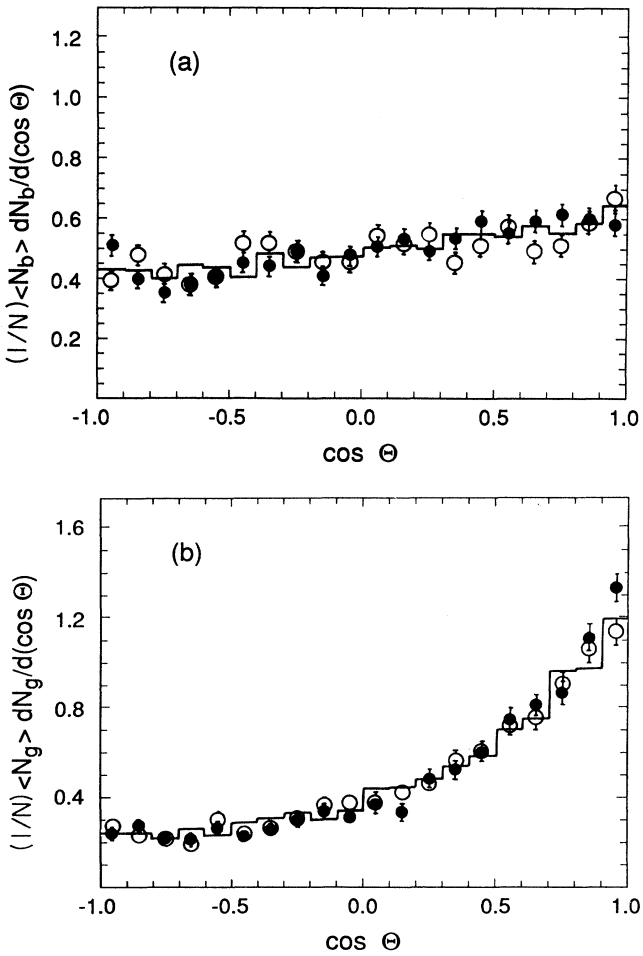

FIG. 15. The angular distribution of (a) black N_b tracks and (b) grey N_g tracks for oxygen (○) and sulfur (●) interactions. For comparison the distribution for proton interactions is shown by the histogram.

TABLE V. The mean values $\langle N_g \rangle$ of grey and $\langle N_b \rangle$ of black tracks for oxygen, sulfur, and proton interactions in emulsion at 200 GeV/nucleon.

Projectile	$\langle N_g \rangle$	$\langle N_b \rangle$
^{16}O	3.9 ± 0.2	4.8 ± 0.2
^{32}S	3.6 ± 0.2	5.1 ± 0.2
p	2.6 ± 0.1	5.0 ± 0.2

of the mass of the projectile. The small differences in the distributions between the proton and heavy nuclei projectiles can be explained by the different relative cross sections of these projectiles on the different groups of nuclei which are the components of nuclear emulsion.

The behavior of grey tracks differs from that of black tracks. Although the multiplicity distributions of grey tracks for oxygen and sulfur projectiles are practically the same, the tails of the distributions are longer than that for proton interactions. Thus the mean values of the N_g distributions for oxygen and sulfur projectiles agree with each other within statistical errors, but are significantly higher than for protons (see Table V).

The angular distributions of grey and black tracks are plotted in Fig. 15. The shapes of the angular distributions of black tracks are the same for proton, oxygen, and sulfur projectiles, and there is no evidence for the sharp decrease in probability at backward angles reported by [26]. As stated in [26], the slight angular dependence for the black tracks suggests that they could well be emitted isotropically from a moving frame of reference with the velocity $\beta = 0.01$.

The angular distributions of grey tracks, as is the case with black tracks, are the same for all projectiles. However, they are strongly peaked forward compared to the black tracks.

The differences in the multiplicity and the angular distributions of grey and black tracks point to the fact that these particles originate in two different processes: the initial interaction, and the subsequent evaporation of the excited target nucleus. The fact that the angular distributions are independent of the type of projectile indicates that the mechanism of slow particle production is identical in all cases, irrespective of the number of intranuclear nucleon-nucleon collisions.

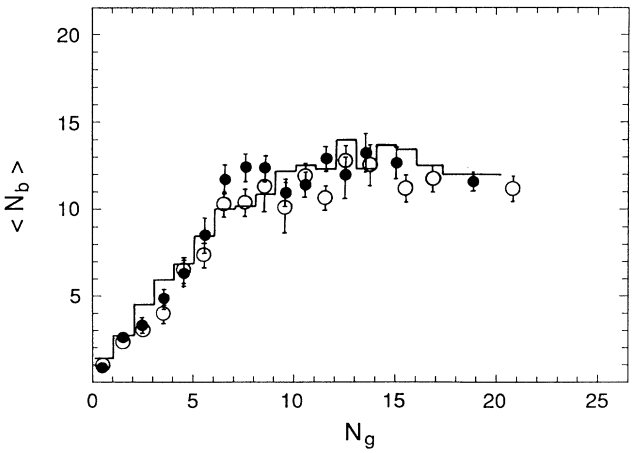

FIG. 16. The dependence of the mean number $\langle N_b \rangle$ of black tracks on the number N_g of grey tracks, for oxygen (○) and sulfur (●) interactions. For comparison the dependence for proton interactions is shown by the histogram.

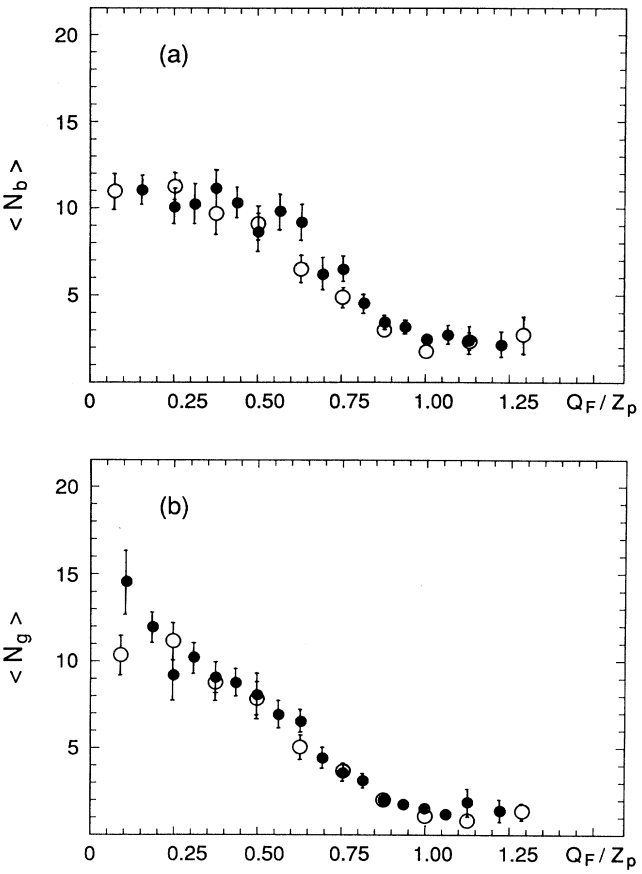

FIG. 17. The dependence of (a) $\langle N_b \rangle$ and (b) $\langle N_g \rangle$ on the normalized forward charge Q_F/Z_P for oxygen (○) and sulfur (●) interactions.

A similar conclusion can be drawn from the correlation between the numbers of black and grey tracks shown in Fig. 16. Again, the oxygen and sulfur data are very similar both to one another and to that observed from the earlier analysis of proton-nucleus interactions [20,21]. Hence this correlation is essentially independent of the mass of the projectile. For $N_g \leq 7$ there is a strong positive correlation in Fig. 16, but for larger values of N_g, the mean value of N_b levels off at a constant value of about 12, independent of the type of projectile.

It was shown in an analysis of oxygen interactions [26] that the mean values of N_g as well as N_b for interactions at 14.6, 60, and 200 GeV/nucleon scale as a function of Q_F. In Fig. 17 $\langle N_g \rangle$ and $\langle N_b \rangle$ are plotted for both oxygen and sulfur projectiles at 200 GeV/nucleon as a function of Q_F/Z_P. In this representation, the $\langle N_g \rangle$ and $\langle N_b \rangle$ values scale for the two different projectiles. The mean value of N_g increases almost linearly with decreasing values of Q_F (i.e., increasing centrality of the collision), while the

$\langle N_b \rangle$ value for central collisions with AgBr nuclei (i.e., for small values of Q_F) becomes constant.

VIII. CONCLUSIONS

Interactions of oxygen and sulfur ions at 200 GeV/nucleon with nuclei of emulsion were investigated and compared with proton-emulsion interactions at the same primary energy. It was found for inclusive data samples that the mean multiplicity $\langle N_\pi \rangle$ of produced particles increases linearly with the increasing number $\langle N_{\rm coll} \rangle$ of intranuclear nucleon-nucleon collisions. The same dependence, except for the largest values of $N_{\rm coll}$, holds when the inclusive data are divided into subsamples characterized by different degrees of centrality. This implies that the multiplicity $\langle N_\pi \rangle$ depends on $\langle N_{\rm coll} \rangle$, and not on the projectile mass. A more detailed analysis performed on the peudorapidity distributions has shown that the linear dependence of $\langle N_\pi \rangle$ on $\langle N_{\rm coll} \rangle$ holds for each particular pseudorapidity interval. We have further found that the normalized particle multiplicity (i.e., the ratio of particles produced in nucleus-nucleus interactions to that in proton-proton interactions) is a function of the number of collisions only and depends neither on the mass of the projectile nor on its energy. In addition, we find that the angular distributions of slow particles emitted from the target nucleus are also independent of the particle mass. All of these results strongly support interaction models in which hadron-nucleus and nucleus-nucleus interactions are considered as an incoherent superposition of intranuclear nucleon-nucleon collisions.

ACKNOWLEDGMENTS

We would like to express our thanks to the technical staff involved in the heavy ion emulsion experiments at CERN for their great help in the preparation of the experiment and during the exposure. We are very indebted to L. H. Bokova for the development of emulsion pellicles. The skillful work of our scanning team is greatly appreciated. This work has been supported in Poland by KBN Grant No. 203799101 and in the U.S. by NSF Grants Nos. PHY-8907660 and INT-8913051 at Louisiana State University and by DOE Grant No. DE-FG02-89ER40528 at University of Minnesota.

[1] J. Bartke, Int. J. Mod. Phys. A **4**, 1319 (1989), and references therein.
[2] *Quark Matter '90*, Proceedings of the 8th International Conference on Ultrarelativistic Nucleus-Nucleus Collisions, Menton, France, 1990, edited by J.P. Blaizot *et al.* [Nucl. Phys. **A525** (1991)].
[3] E.V. Shuryak, Phys. Rep. **115**, 151 (1984).
[4] J.B. Kogut, in *Quark Matter '83*, Proceedings of the Third International Conference on Ultrarelativistic Nucleus-Nucleus Collisions, Upton, New York, 1983, edited by T.W. Ludlam and H. Wegner [Nucl. Phys. **A418**, 381c (1984)].
[5] H. Satz, in *Quark Matter '83* [4], p. 447c.
[6] H. Satz, Annu. Rev. Nucl. Part. Sci. **35**, 245 (1985).
[7] B. Muller, *The Physics of the Quark-Gluon Plasma*, Lecture Notes in Physics Vol. 225 (Springer, Berlin, 1985).
[8] A. Bialas and R. Peschanski, Nucl. Phys. **B273**, 70 (1986).
[9] R. Holynski *et al.*, Phys. Rev. Lett. **62**, 733 (1989).
[10] R. Holynski *et al.*, Phys. Rev. C **40**, 2449 (1989).
[11] B. Wosiek, Krakow Institute of Nuclear Physics Report No. 1533/PH, 1991 (unpublished).
[12] E. Stenlund and I. Otterlund, Nucl. Phys. **B198**, 407 (1982).
[13] R. Holynski *et al.*, Z. Phys. C **31**, 467 (1986).
[14] S. Fredriksson *et al.*, Phys. Rep. **144**, 187 (1987).
[15] K. Werner, Phys. Rev. D **39**, 780 (1989); CERN Report No. CERN-TH 5682, 1990 (unpublished).
[16] B. Andersson *et al.*, Nucl. Phys. **B281**, 289 (1987).
[17] G.D. Westfall *et al.*, Phys. Rev. C **19**, 1309 (1979).
[18] F. Hagen, Ph.D. thesis, University of Maryland, 1976.
[19] L.H. Bokova (private communication).
[20] J. Babecki *et al.*, Phys. Lett. **47B**, 268 (1973).
[21] A. Azimov *et al.*, Yad. Fiz. **22**, 736 (1975) [Sov. J. Nucl. Phys. **22**, 380 (1975)].
[22] M.I. Adamovich *et al.*, Phys. Lett. B **223**, 262 (1989).
[23] M.I. Adamovich *et al.*, Phys. Rev. Lett. **62**, 280 (1989).
[24] J.B. Andersson *et al.*, Phys. Lett. **73B**, 343 (1978).
[25] J.E. Elias *et al.*, Phys. Rev. D **22**, 13 (1980).
[26] M.I. Adamovich *et al.*, Report No. LUIP 9103, 1991 (unpublished).
[27] H. von Gersdorff *et al.*, Phys. Rev. C **39**, 1385 (1989).
[28] C.J. Waddington *et al.*, in *Proceedings of the 21st International Cosmic Ray Conference*, Adelaide, Australia, 1989, edited by R. J. Protheroe (Graphic Services, Northfield, South Australia, 1990), Vol. 8, p. 87.
[29] N.P. Andreeva *et al.*, Yad. Fiz. **47**, 157 (1988) [Sov. J. Nucl. Phys. **47**, 102 (1988)].
[30] C.J. Waddington and P.S. Freier, Phys. Rev. C **31**, 888 (1985).